Reconstruction of Non-Cartesian MRI Data

Friedrich-Alexander-Universität
Computational Imaging Lab

NYU

K-space

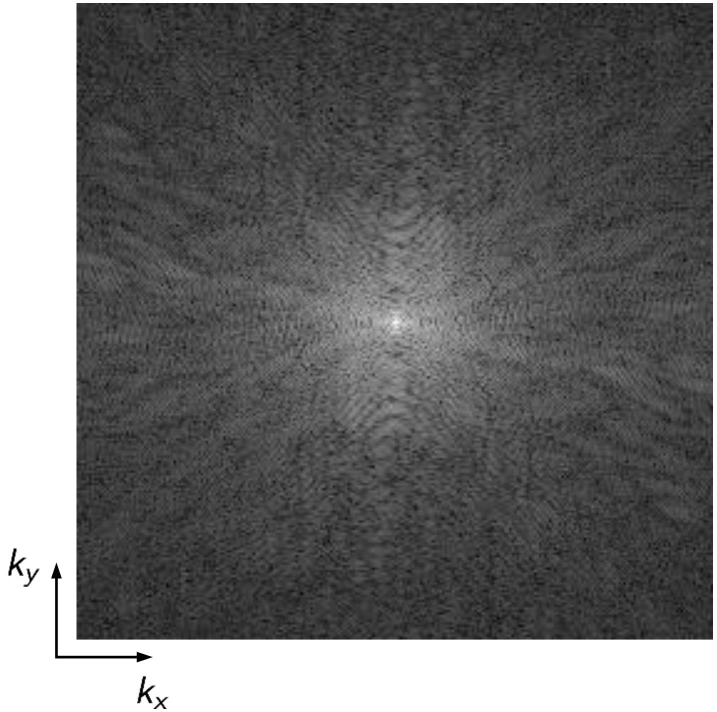

$$\xrightarrow{\mathcal{FT}^{-1}}$$

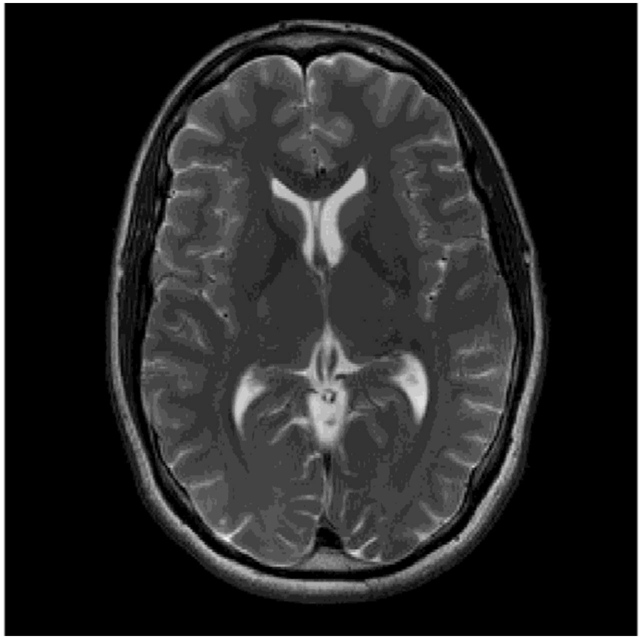

Gradient fields and K-space

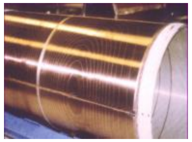

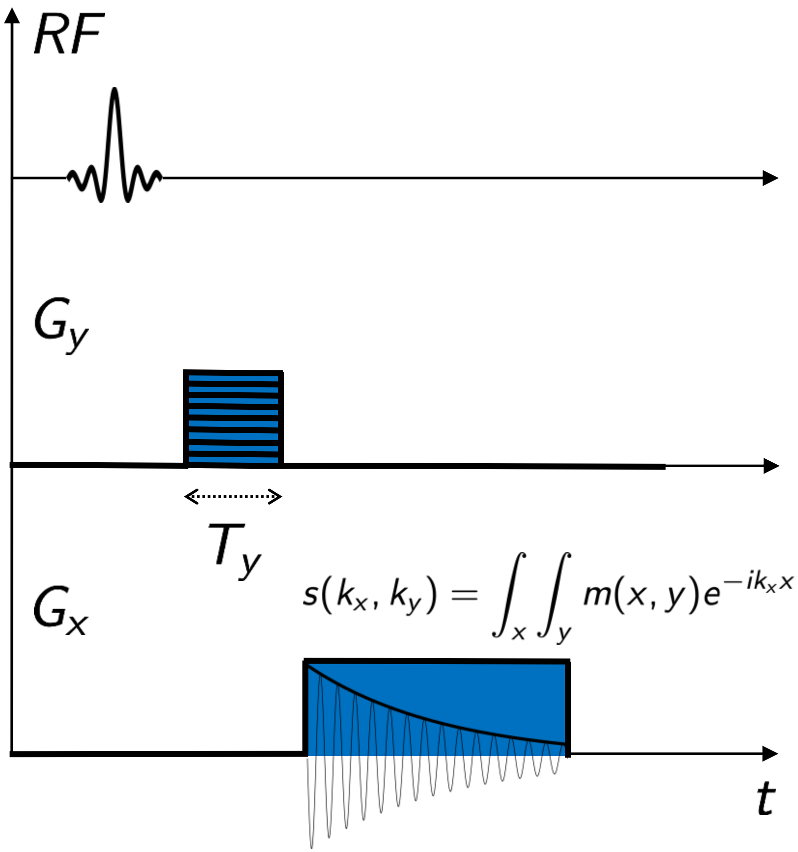

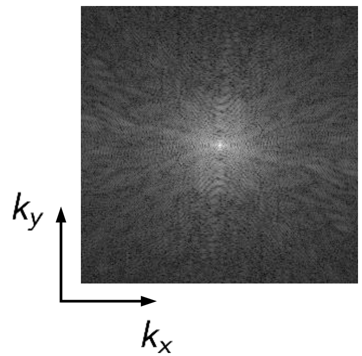

$$\xrightarrow{\mathcal{FT}^{-1}}$$

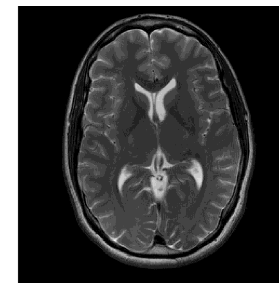

$$s(k_x, k_y) = \int_x \int_y m(x, y) e^{-ik_x x} e^{-ik_y y} \, dxdy$$

$$\phi(x, t) = \gamma x \int_0^t G_x d\tau \equiv k_x x$$

$$\phi(y, G_y) = \gamma y \int_0^{T_y} G_y d\tau \equiv k_y y$$

Non-Cartesian MRI

Radial

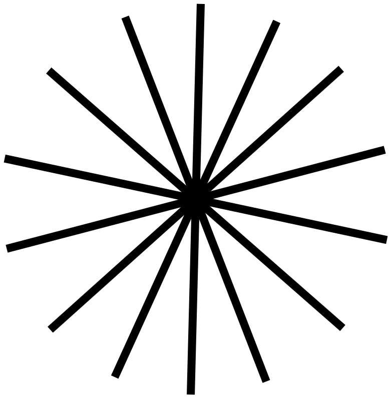

EPI

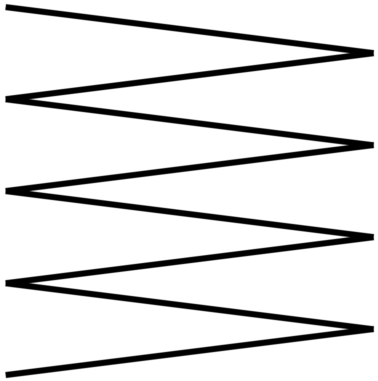

Spiral

- Pros: fast, motion-robust, self-navigation
- Cons: Susceptible to hardware imperfections (off-resonance, gradient linearity, eddy currents)
- Cons: Numerically more challenging reconstruction

Reconstruction of non-Cartesian MRI data

- Direct FFT does not work

- In general
  - DFT: Compute the inverse Fourier transform according to the trajectory (slow)
  - Gridding: resample the non-Cartesian MRI data into a Cartesian grid and apply inverse FFT (fast)

- Radial MRI
  - Backprojection reconstruction, like in CT

Filtered backprojection reconstruction (CT)

Original MRI experiment

Image Formation by Induced Local Interactions: Examples Employing Nuclear Magnetic Resonance

AN image of an object may be defined as a graphical representation of the spatial distribution of one or more of its properties. Image formation usually requires that the object interact with a matter or radiation field characterized by a wavelength comparable to or smaller than the smallest features to be distinguished, so that the region of interaction may be restricted and a resolved image generated.

This limitation on the wavelength of the field may be removed, and a new class of image generated, by taking advantage of induced local interactions. In the presence of a second field that restricts the interaction of the object with the first field to a limited region, the resolution becomes independent of wavelength, and is instead a function of the ratio of the normal width of the interaction to the shift produced by a gradient in the second field. Because the interaction may be regarded as a coupling of the two fields by the object, I propose that image formation by this technique be known as zeugmatography, from the Greek ζευγμα, "that which is used for joining".

The nature of the technique may be clarified by describing two simple examples. Nuclear magnetic resonance (NMR) zeugmatography was performed with 60 MHz (5 m) radiation and a static magnetic field gradient corresponding, for proton resonance, to about 700 Hz cm^{-1}. The test object consisted of two 1 mm inside diameter thin-walled glass capillaries of H_2O attached to the inside wall of a 4.2 mm inside diameter glass tube of D_2O. In the first experiment, both capillaries contained pure water. The proton resonance line width, in the absence of the transverse field gradient, was about 5 Hz. Assuming uniform signal strength across the region within the transmitter–receiver coil, the signal in the presence of a field gradient represents a one-dimensional projection of the H_2O content of the object, integrated over planes perpendicular to the gradient direction, as a function of the gradient coordinate (Fig. 1). One method of constructing a two-dimensional projected image of the object, as represented by its H_2O content, is to combine several projections, obtained by rotating the object about an axis perpendicular to the gradient direction (or, as in Fig. 1, rotating the gradient about the object), using one of the available methods for reconstruction of objects from their projections[1–5]. Fig. 2 was generated by an algorithm, similar to that of Gordon and Herman[4], applied to four projections, spaced as in Fig. 1, so as to construct a 20×20 image matrix. The representation shown was produced by shading within contours interpolated between the matrix points, and clearly reveals the locations and dimensions of the two columns of H_2O. In the second experiment, one capillary contained pure H_2O, and the other contained a 0.19 mM solution of $MnSO_4$ in H_2O. At low radio-frequency power (about 0.2 mgauss) the two capillaries gave nearly identical images in the

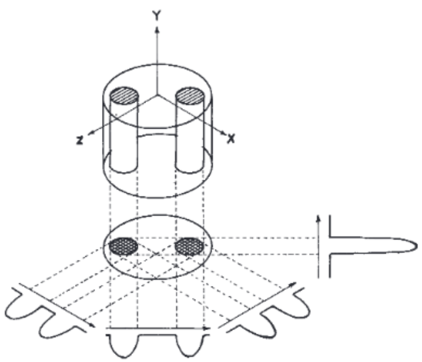

Fig. 1 Relationship between a three-dimensional object, its two-dimensional projection along the Y-axis, and four one-dimensional projections at 45° intervals in the XZ-plane. The arrows indicate the gradient directions.

Fig. 2 Proton nuclear magnetic resonance zeugmatogram of the object described in the text, using four relative orientations of object and gradients as diagrammed in Fig. 1.

zeugmatogram (Fig. 3*a*). At a higher power level (about 1.6 mgauss), the pure water sample gave much more saturated signals than the sample whose spin-lattice relaxation time T_1 had been shortened by the addition of the paramagnetic Mn^{2+} ions, and its zeugmatographic image vanished at the contour level used in Fig. 3*b*. The sample region with long T_1 may be selectively emphasized (Fig. 3*c*) by constructing a difference zeugmatogram from those taken at different radio-frequency powers.

Applications of this technique to the study of various inhomogeneous objects, not necessarily restricted in size to those commonly studied by magnetic resonance spectroscopy, may be anticipated. The experiments outlined above demonstrate the ability of the technique to generate pictures of the distributions of stable isotopes, such as H and D, within an object. In the second experiment, relative intensities in an image were made to depend upon relative nuclear relaxation times. The variations in water contents and proton relaxation times among biological tissues should permit the generation, with field gradients large compared to internal magnetic inhomogeneities, of useful zeugmatographic images from the rather sharp water resonances of organisms, selectively picturing the various soft structures and tissues. A possible application of considerable interest at this time would be to the *in vivo* study of malignant tumours, which have been shown to give proton nuclear magnetic resonance signals with much longer water spin-lattice relaxation times than those in the corresponding normal tissues[6].

The basic zeugmatographic principle may be employed in many different ways, using a scanning technique, as described above, or transient methods. Variations on the experiment, to be described later, permit the generation of two- or three-dimensional images displaying chemical compositions, diffusion coefficients and other properties of objects measurable by spectroscopic techniques. Although applications employing nuclear magnetic resonance in liquid or liquid-like systems are simple and attractive because of the ease with which field gradients large enough to shift the narrow resonances by many line widths may be generated, NMR zeugmatography of solids, electron spin resonance zeugmatography, and analogous experiments in other regions of the spectrum should also be possible. Zeugmatographic techniques should find many useful applications in studies of the internal structures, states, and compositions of microscopic objects.

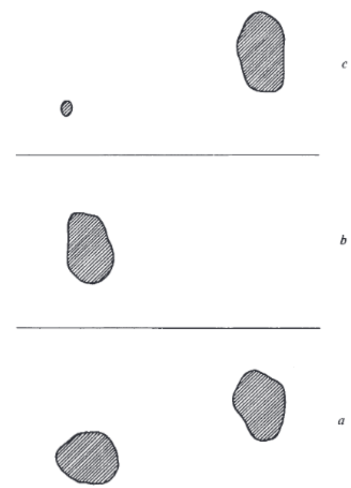

Fig. 3 Proton nuclear magnetic resonance zeugmatograms of an object containing regions with different relaxation times. *a*, Low power; *b*, high power; *c*, difference between *a* and *b*.

P. C. LAUTERBUR

Department of Chemistry,
State University of New York at Stony Brook,
Stony Brook, New York 11790

Received October 30, 1972; revised January 8, 1973.

[1] Bracewell, R. N., and Riddle, A. C., *Astrophys. J.*, **150**, 427 (1967).
[2] Vainshtein, B. K., *Soviet Physics–Crystallography*, **15**, 781 (1971).
[3] Ramachandran, G. N., and Lakshminarayan, A. V., *Proc. US Nat. Acad. Sci.*, **68**, 2236 (1971).
[4] Gordon, R., and Herman, G. T., *Comm. Assoc. Comput. Mach.*, **14**, 759 (1971).
[5] Klug, A., and Crowther, R. A., *Nature*, **238**, 435 (1972).
[6] Weisman, I. D., Bennett, L. H., Maxwell, Sr., L. R., Woods, M. W., and Burk, D., *Science*, **178**, 1288 (1972).

Original MRI experiment

- Radial k-space sampling
- Filtered backprojection reconstruction

Image Formation by Induced Local Interactions: Examples Employing Nuclear Magnetic Resonance

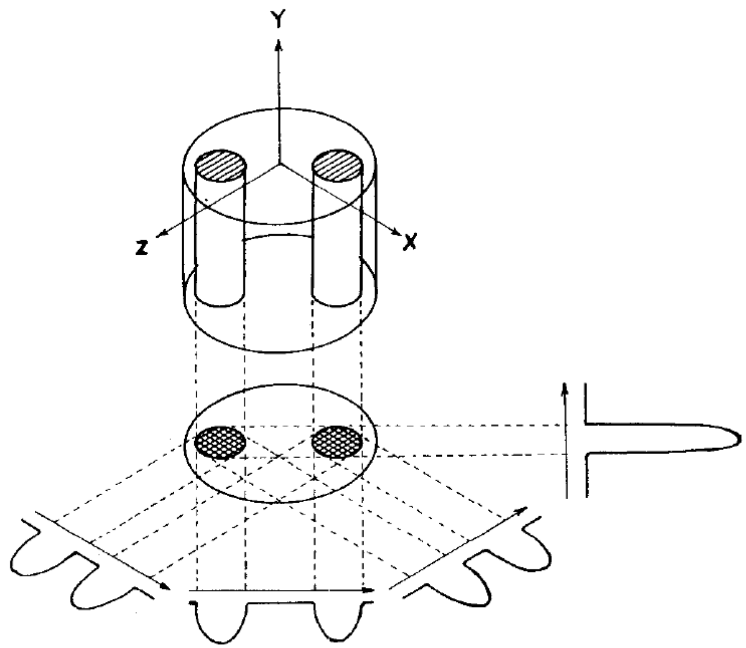

Lauterbur P, Nature 1973

Projections & the Radon transform

- Physical problem: parallel X-rays passing through an object

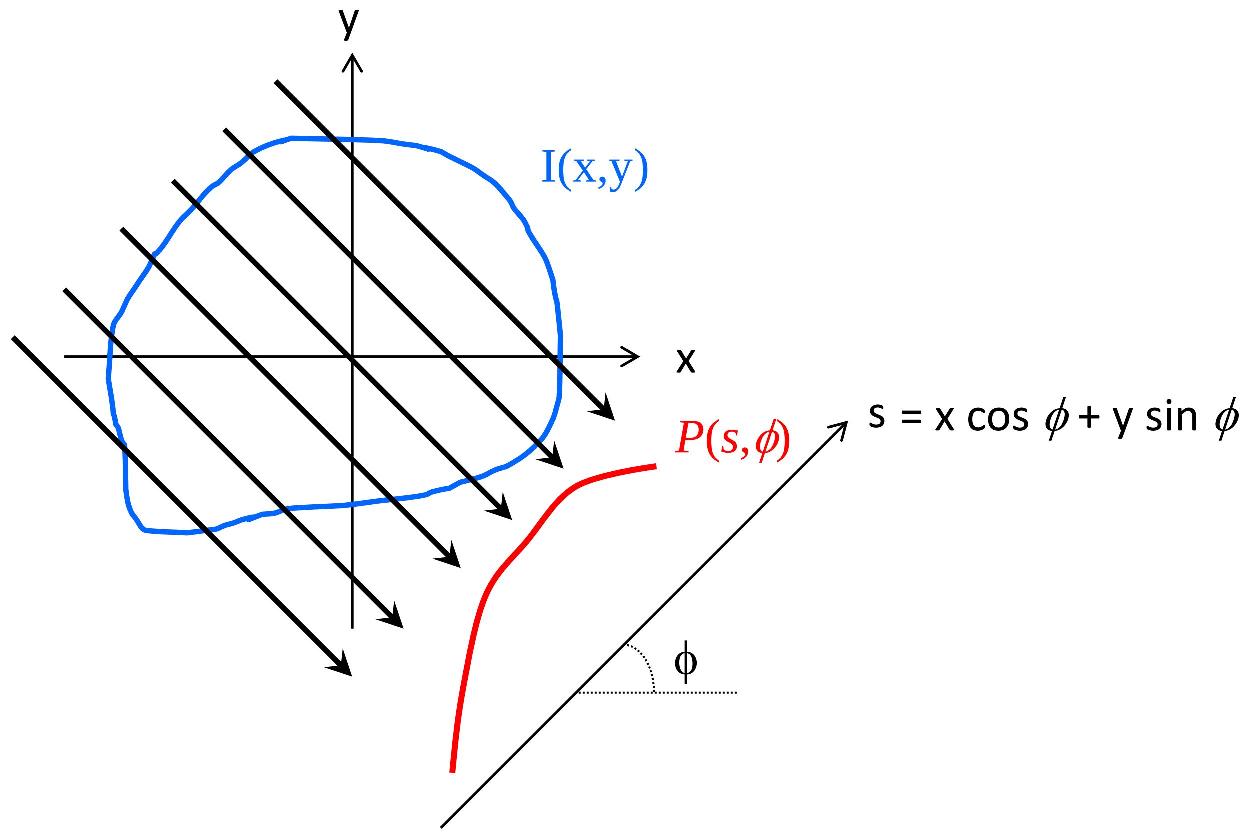

$$P(s,\phi) = \iint_{x,y} I(x,y)\,\delta(x\cos\phi + y\sin\phi - s)\,dx\,dy$$

Projections & the Radon transform

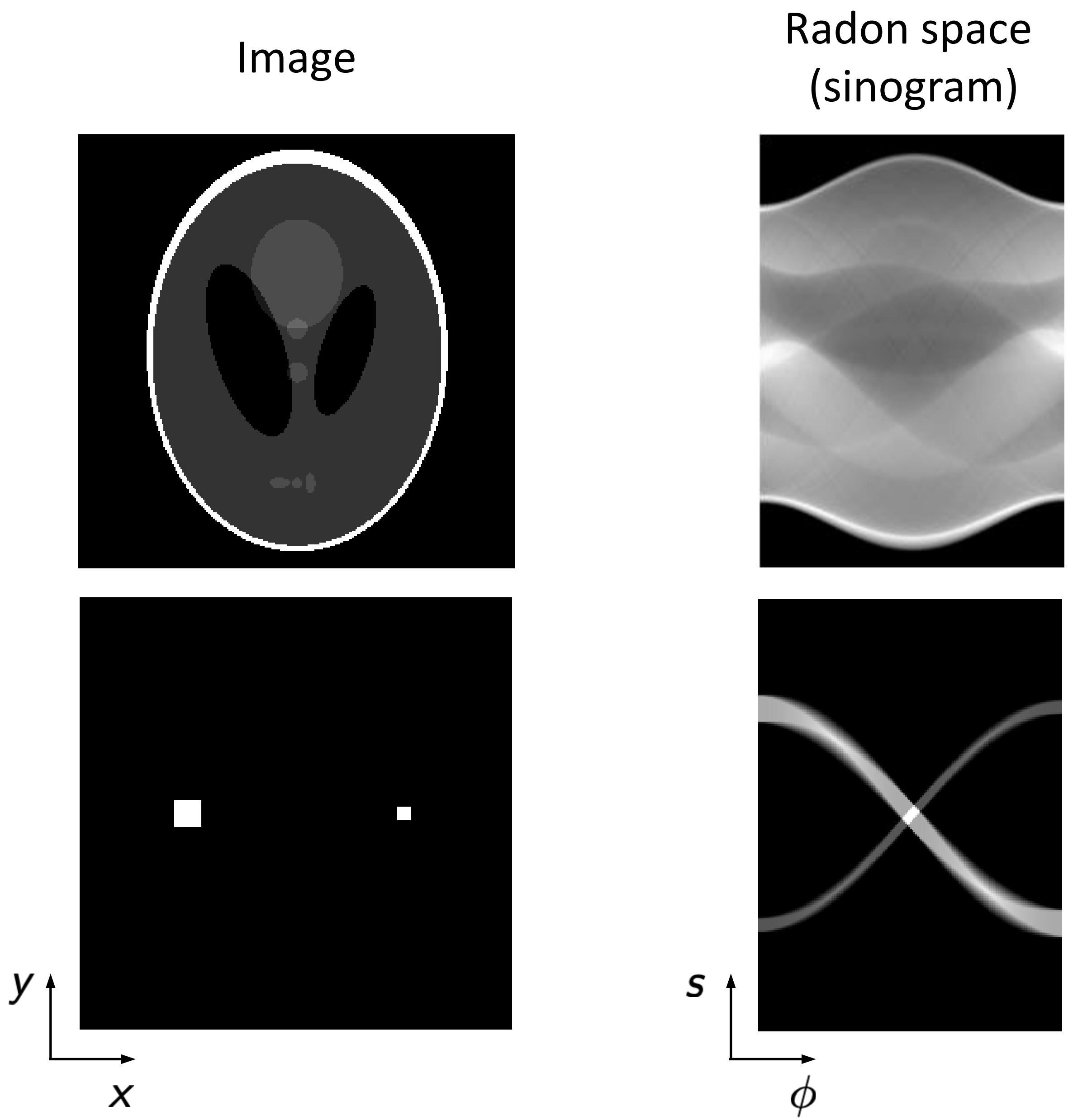

Fourier-slice theorem (a.k.a. central-slice theorem)

- The 1D Fourier transform of the projection at angle ϕ is a radial line in k-space at angle ϕ

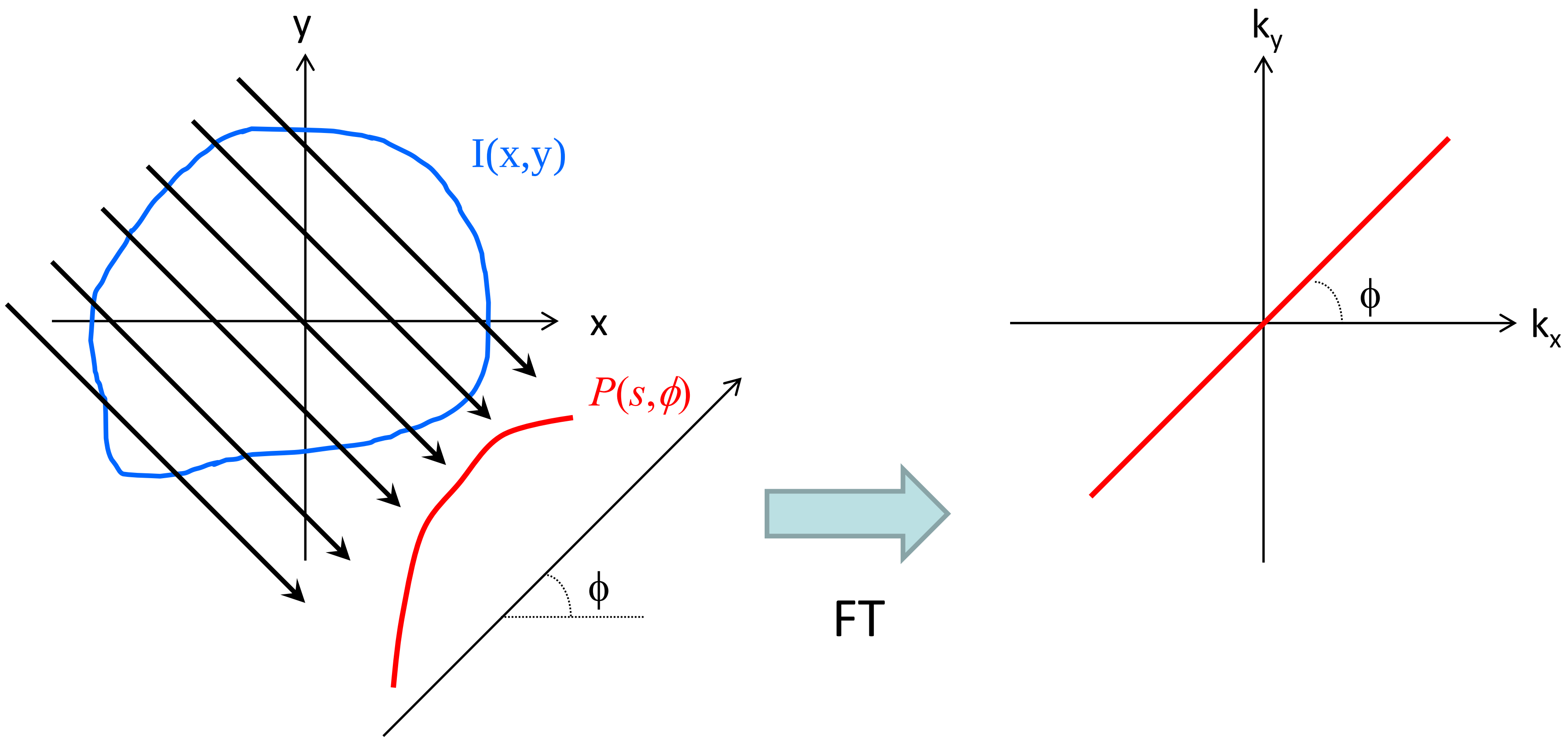

Fourier Slice Theorem: Bracewell (1956)

Backprojection

- Undo the projection
- Push ray through image matrix

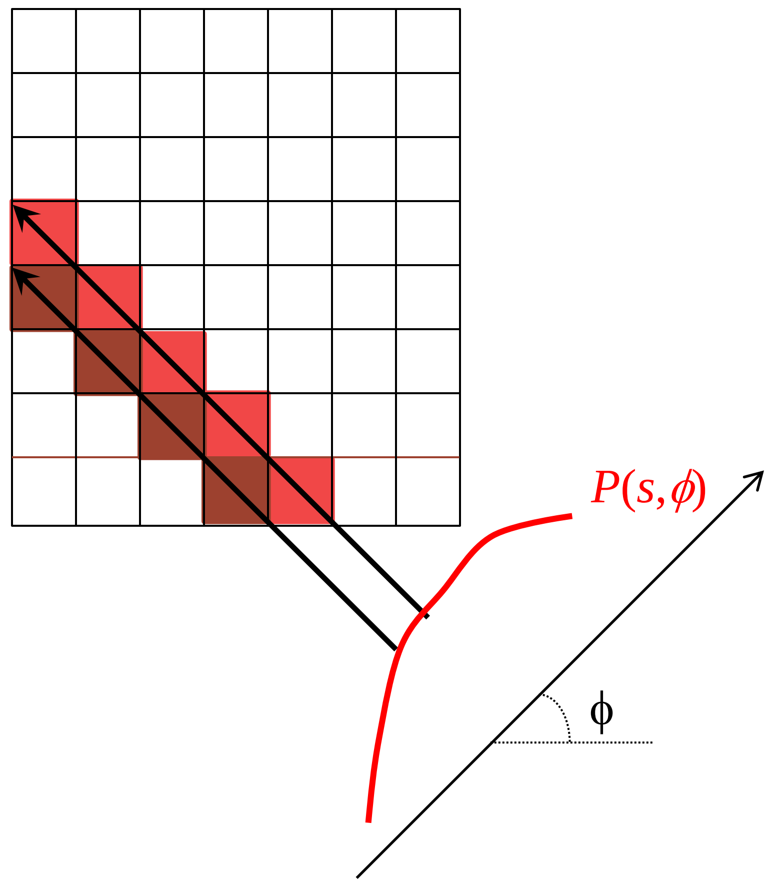

Backprojection

- Accumulate backprojections for all angles

$$b(x_i, y_i) = \sum_{n=1}^{N} P\left(x_i cos(\phi_n) + y_i sin(\phi_n), \phi_n\right)$$

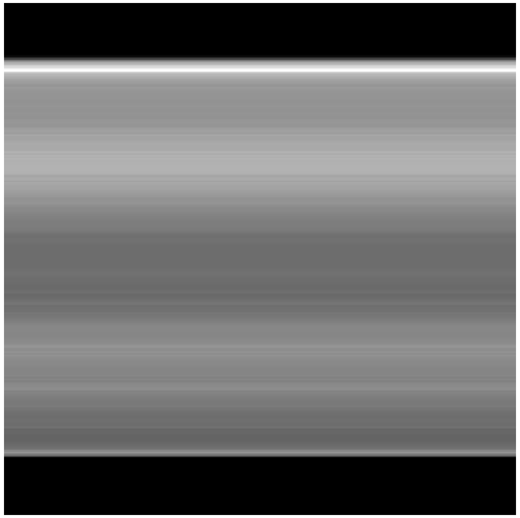

Backprojection

- Straight backprojection leads to blurring

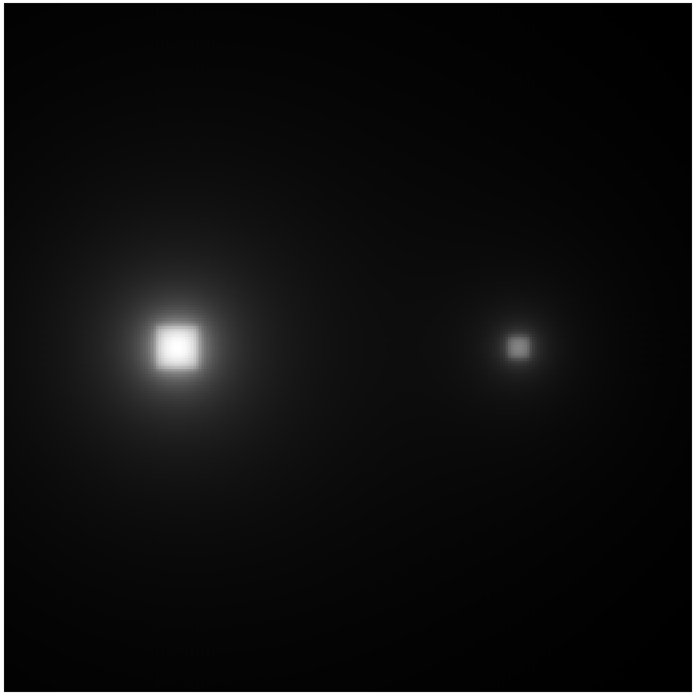

What is wrong?

Backprojection

- Straight backprojection leads to blurring
  - Variable-density sampling in Fourier space (k-space)

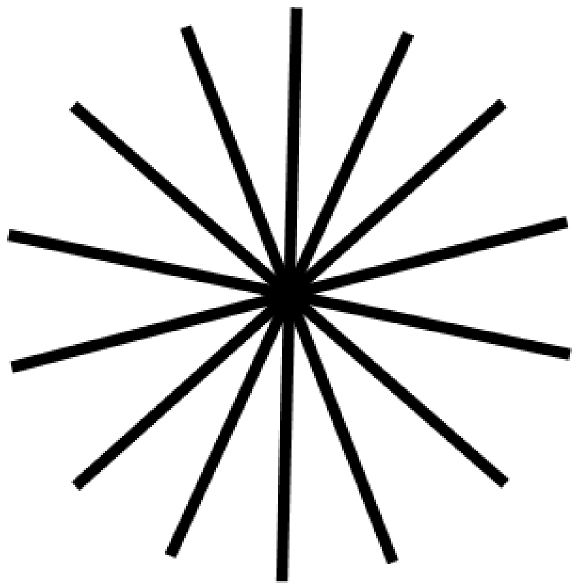

The center is
acquired N times

Filtered backprojection

- Density compensation in k-space
  - Ramp or rho filter

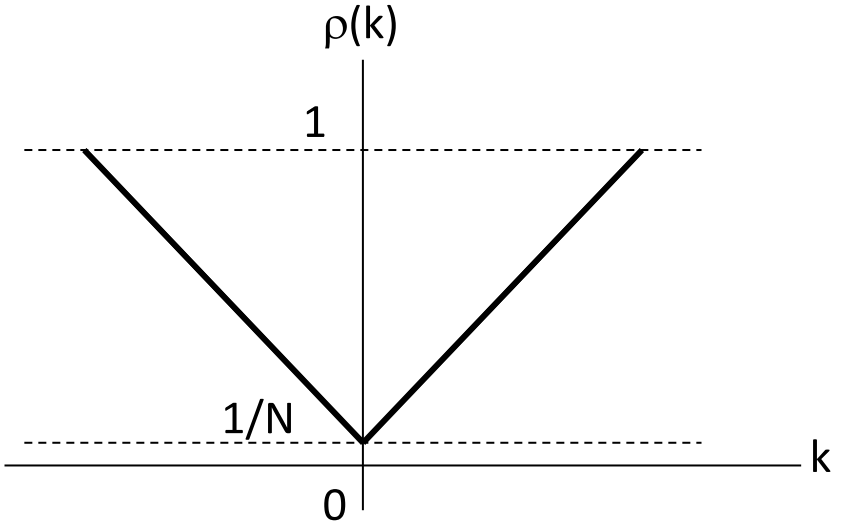

Kak, Slaney. Principles of Computerized Tomographic Imaging (1988)

Filtered backprojection algorithm

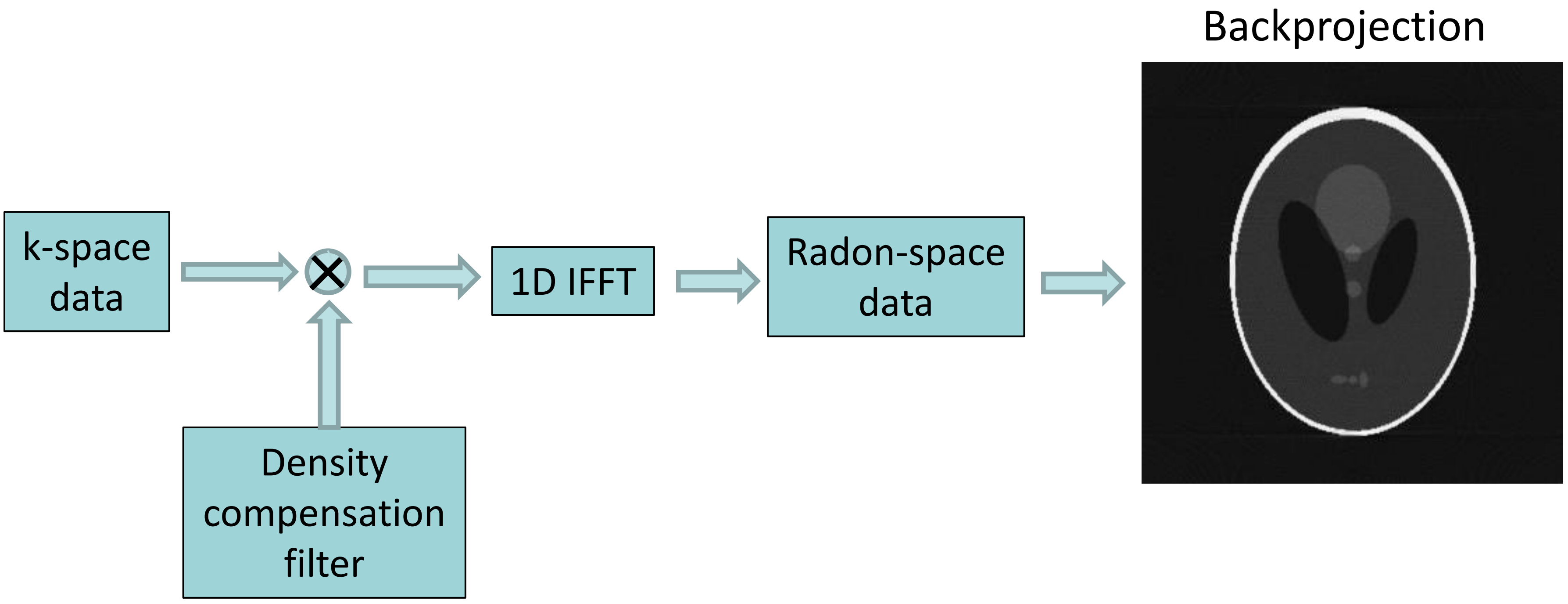

Gridding reconstruction

Gridding

- Faster approach
- Convolution-based interpolation + FFT

Non-Cartesian

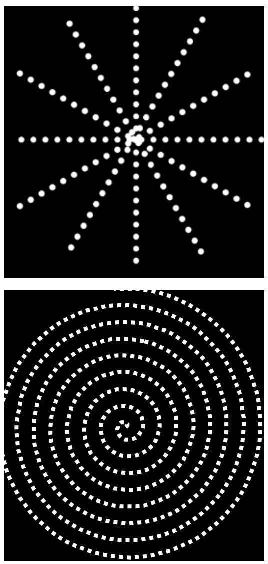

convolve
&
resample

Cartesian

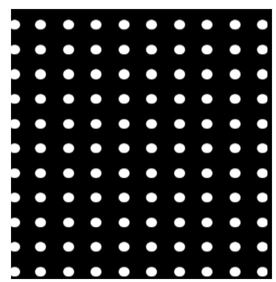

FFT

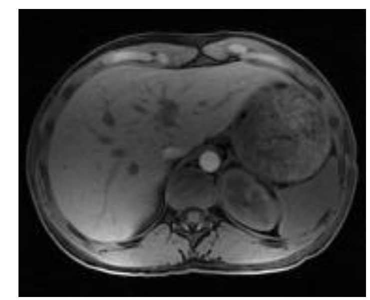

Jackson JI et al. IEEE TMI 1991

Gridding

- Convolve with a k-space kernel
- Evaluate the convolution at the Cartesian grid

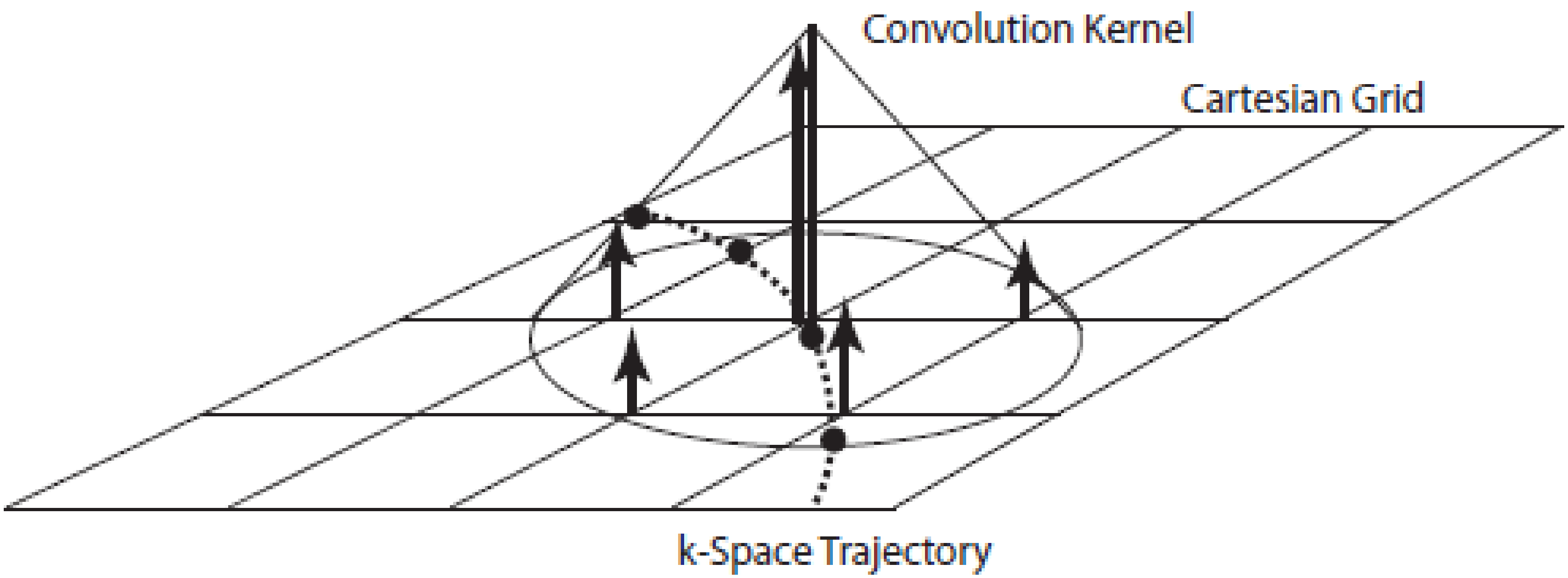

Mathematical description of gridding

- Non-Cartesian sampling function: $S(k_x, k_y) = \sum_i \delta\left(k_x - k_{x,i}, k_y - k_{y,i}\right)$

- Sampled data: $M(k_x, k_y)S(k_x, k_y)$

- Convolution with the gridding kernel and resampling on the Cartesian grid:

$$\widehat{M}(k_x, k_y) = \left[\left(M(k_x, k_y)S(k_x, k_y)\right) * C(k_x, k_y)\right] \times III\left(\frac{k_x}{K_x}, \frac{k_y}{K_y}\right)$$

- After applying the inverse Fourier transform:

$$\hat{m}(x, y) = \left[\left(m(x, y) * s(x, y)\right)c(x, y)\right] * III\left(\frac{x}{FOV_x}, \frac{y}{FOV_y}\right)$$

Effect of gridding operations

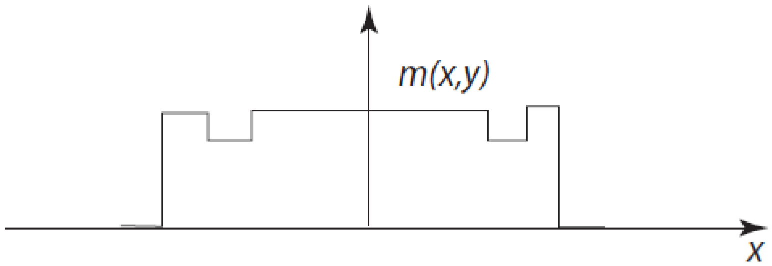

Original signal

Courtesy of John Pauly (Stanford)

Effect of gridding operations

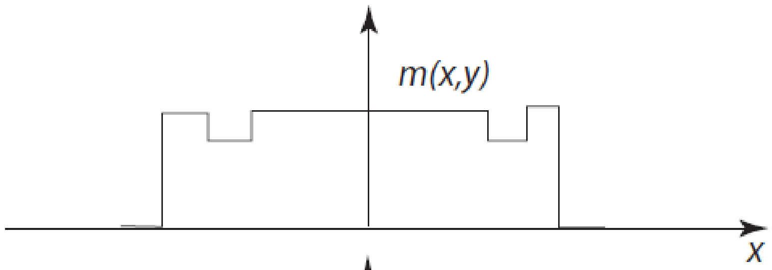

Original signal

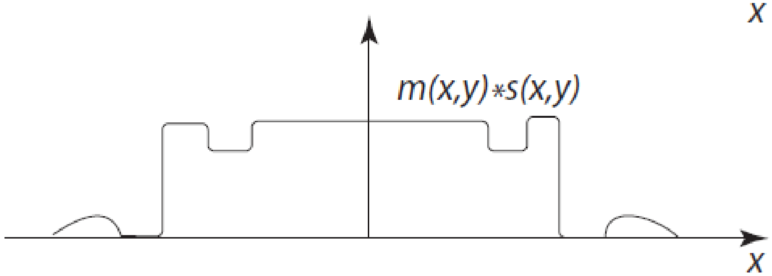

Blurring + side lobes

Courtesy of John Pauly (Stanford)

Effect of gridding operations

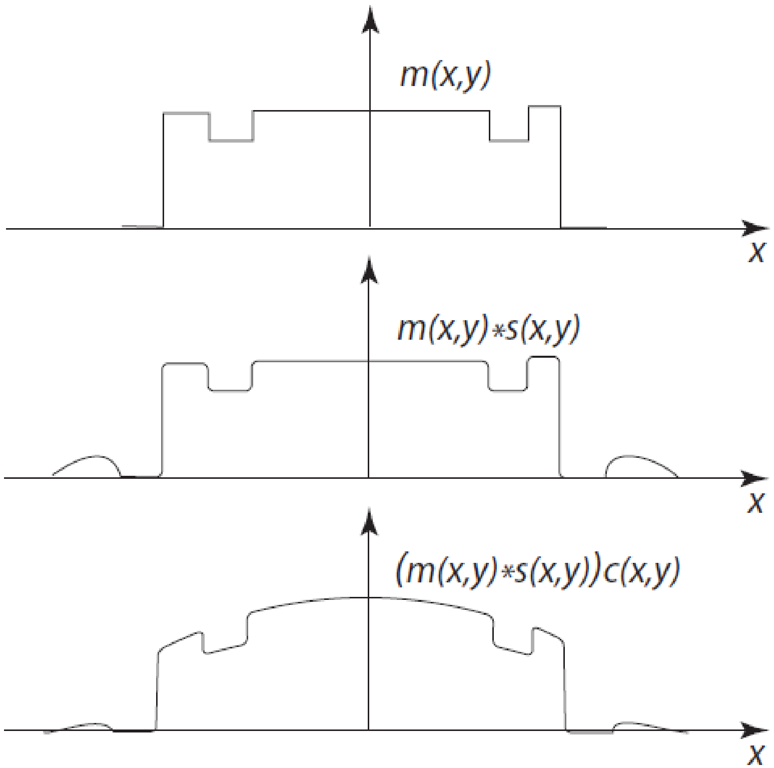

Original signal

Blurring + side lobes

Apodization

Courtesy of John Pauly (Stanford)

Effect of gridding operations

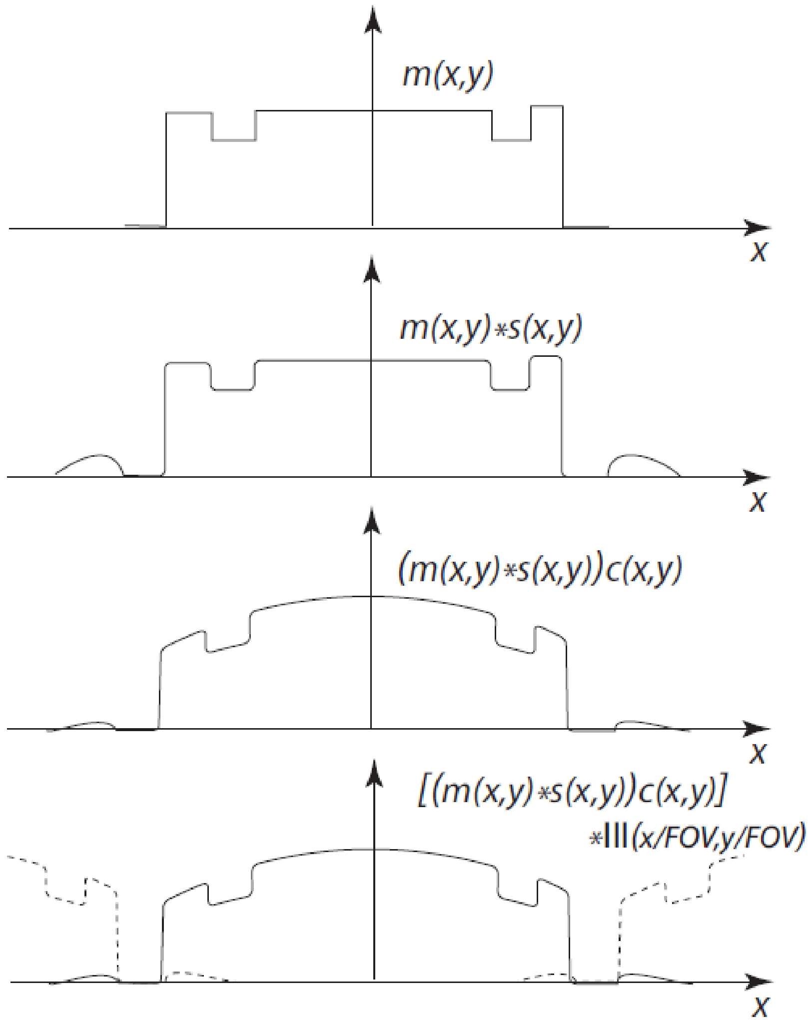

Original signal

Blurring + side lobes

Apodization

Replication

Courtesy of John Pauly (Stanford)

Simple gridding

- 3-point triangular kernel

Radial k-space
200x200 grid

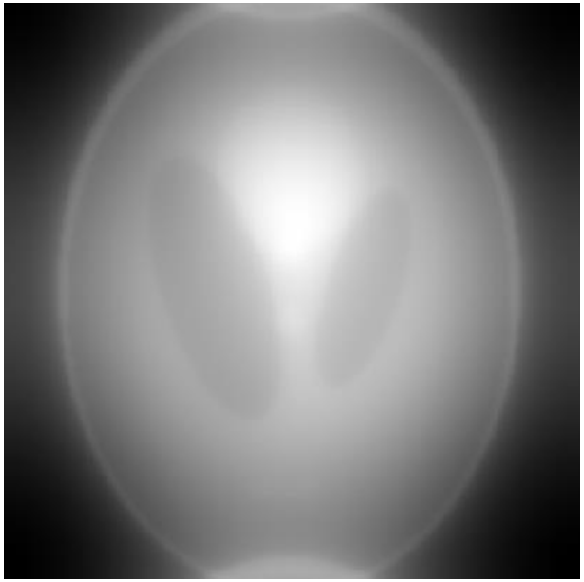

Spiral k-space
128x128 grid

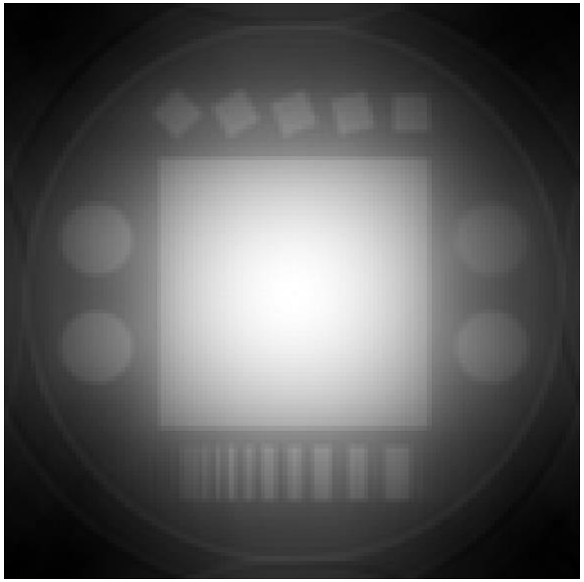

Sampling density compensation

- Non-Cartesian trajectories sample k-space with variable density
  - Radial imaging: the central point is acquired N times

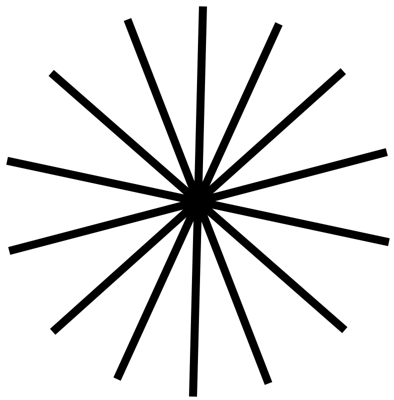

- Non-uniform k-space weighting

Sampling density compensation

- Pre-compensation
  - Sampling density (ρ) must be pre-computed

$$\hat{M}(k_x,k_y)=\left[\left(\frac{M(k_x,k_y)}{\rho(k_x,k_y)}S(k_x,k_y)\right)*C(k_x,k_y)\right]\times III\left(\frac{k_x}{\Delta k_x},\frac{k_y}{\Delta k_y}\right)$$

  - Using geometry

For radial MRI:

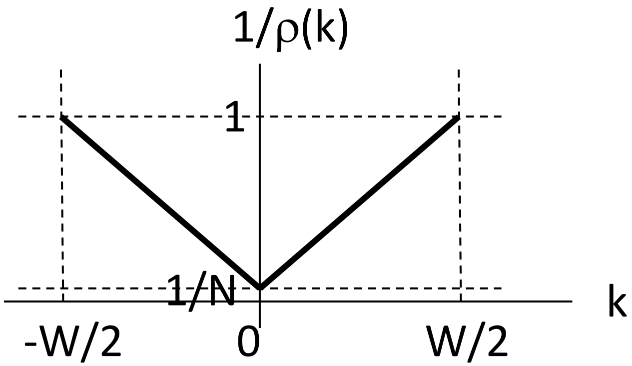

  - Assign an area to each k-space sample (numerical method)
    - E.g. Voronoi diagram

Sampling density compensation

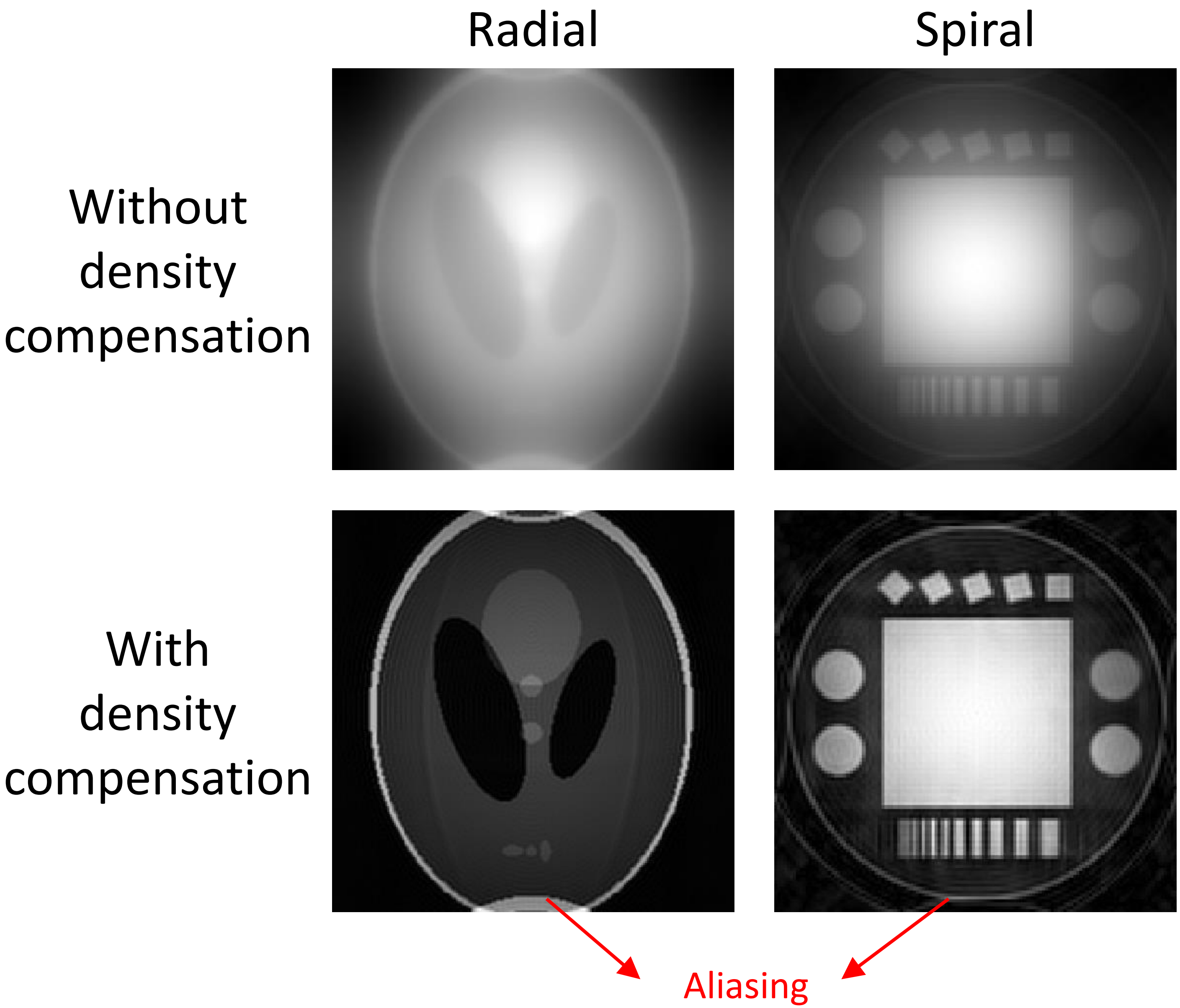

Convolution kernel

- The ideal kernel would be an infinite sinc (impractical)

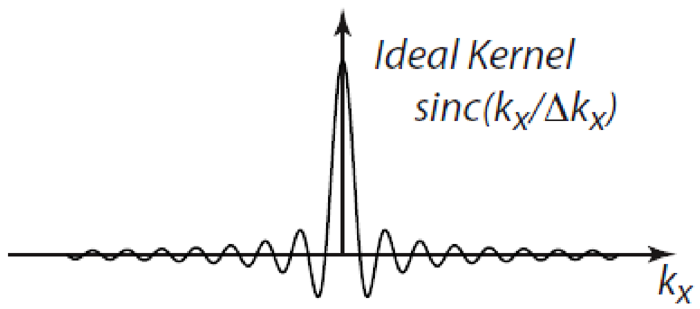

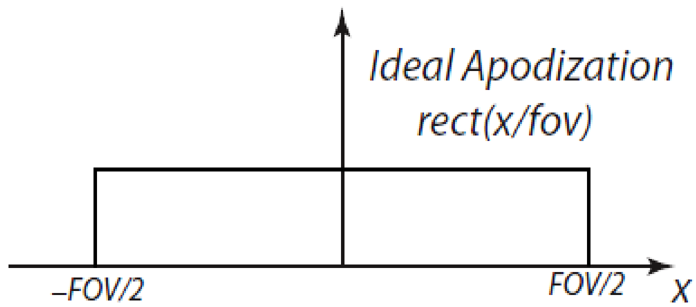

- Windowed sinc

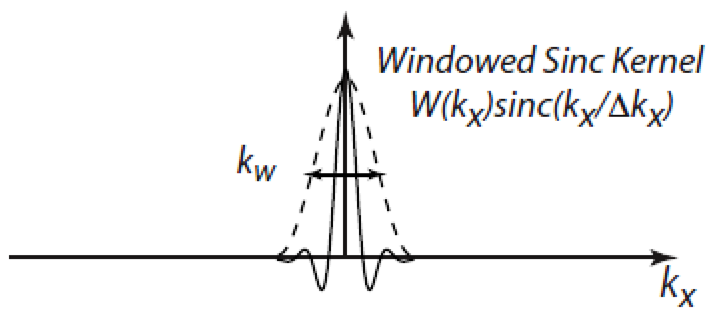

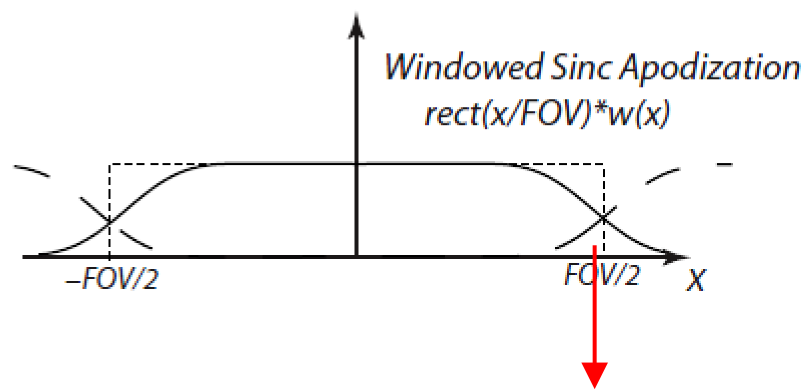

Aliasing

Courtesy of John Pauly (Stanford)

Oversampling the Cartesian grid

- Removes aliasing
- Reduces apodization

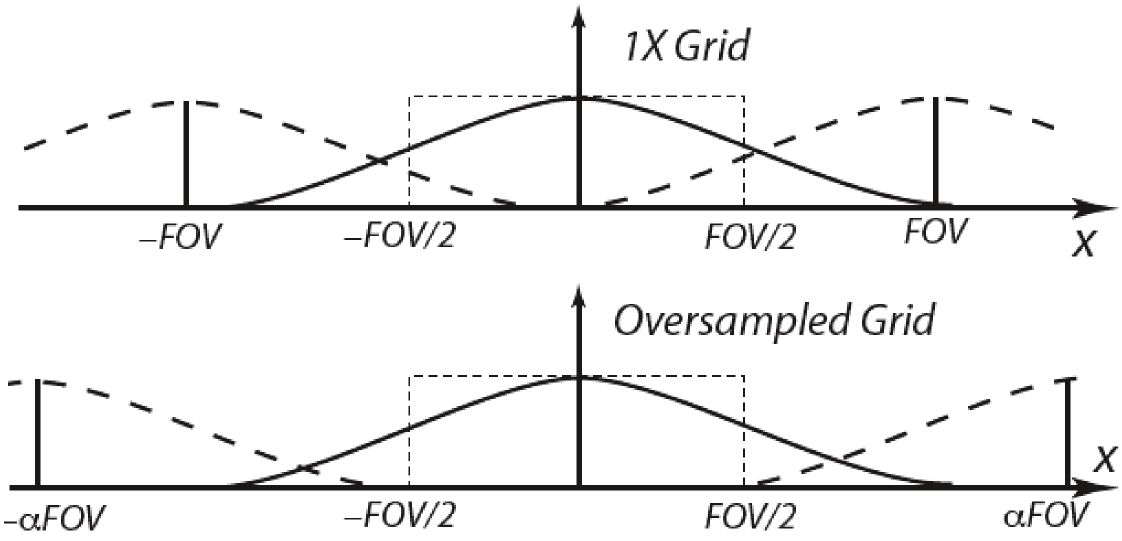

Courtesy of John Pauly (Stanford)

Oversampling the Cartesian grid

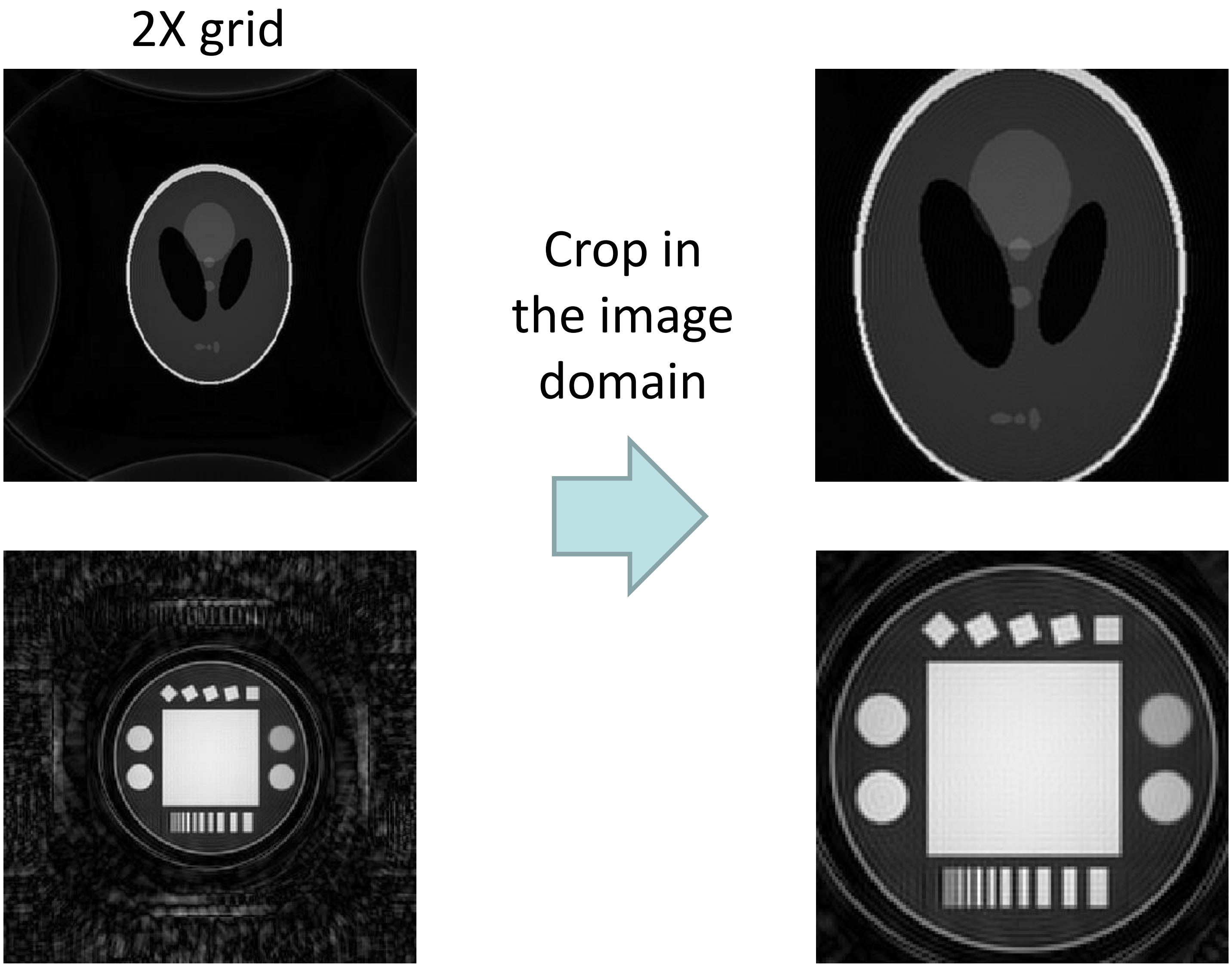

Convolution kernel

- Kaiser-Bessel function
  - Best kernel (by consensus)

$$C(k) = \frac{1}{W} I_0\left(b\left(1 - 2\frac{k}{W}\right)^2 \right) rect\left(\frac{2k}{W}\right)$$

I_0: zero-order modified Bessel function of the first kind
W: width of the kernel
b: scaling parameter

  - Inverse Fourier transform

$$c(x) = \frac{\sin\left(\sqrt{\pi^2 W^2 x^2 - b^2}\right)}{\sqrt{\pi^2 W^2 x^2 - b^2}}$$

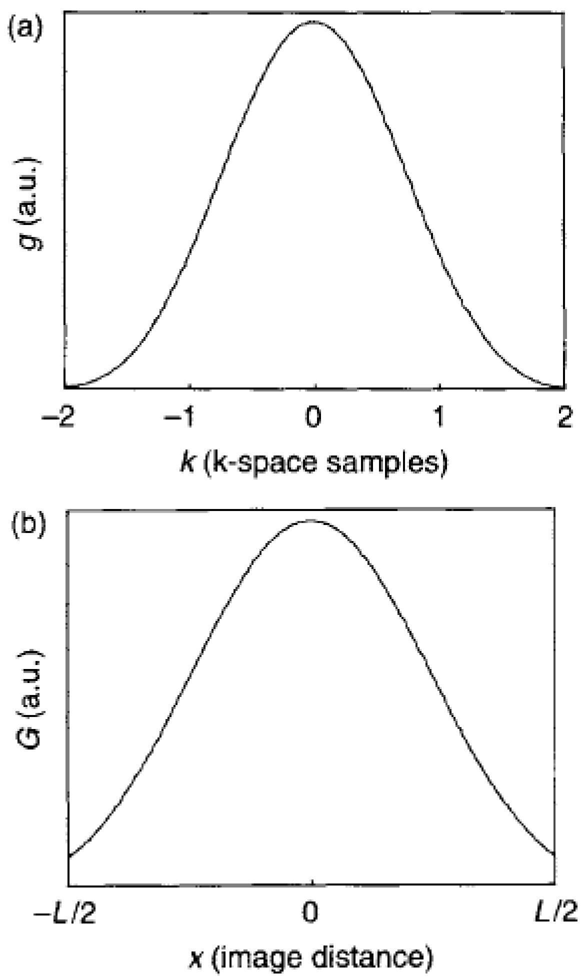

Reconstruction kernel comparison

Triangular | Kaiser-Bessel

1.5X grid

1.25X grid

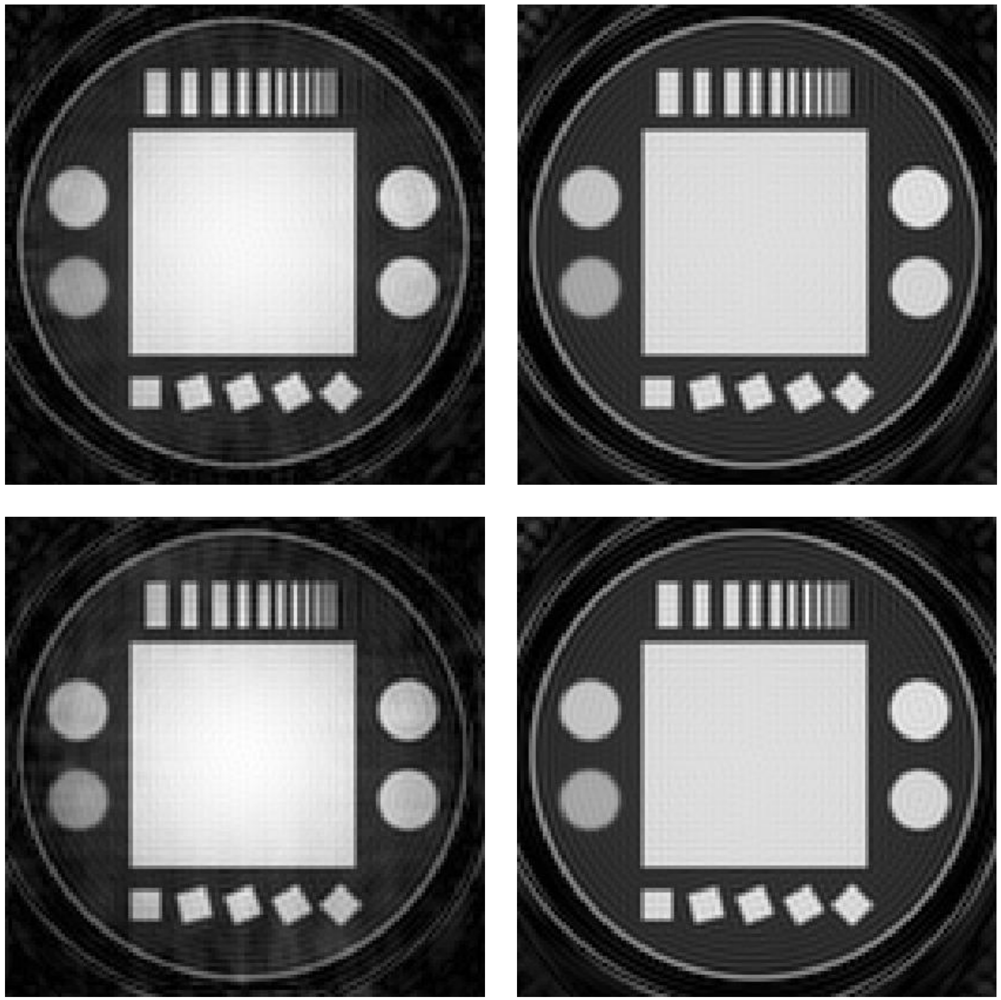

Deapodization

- Divide the reconstructed image by the inverse Fourier transform of the gridding kernel

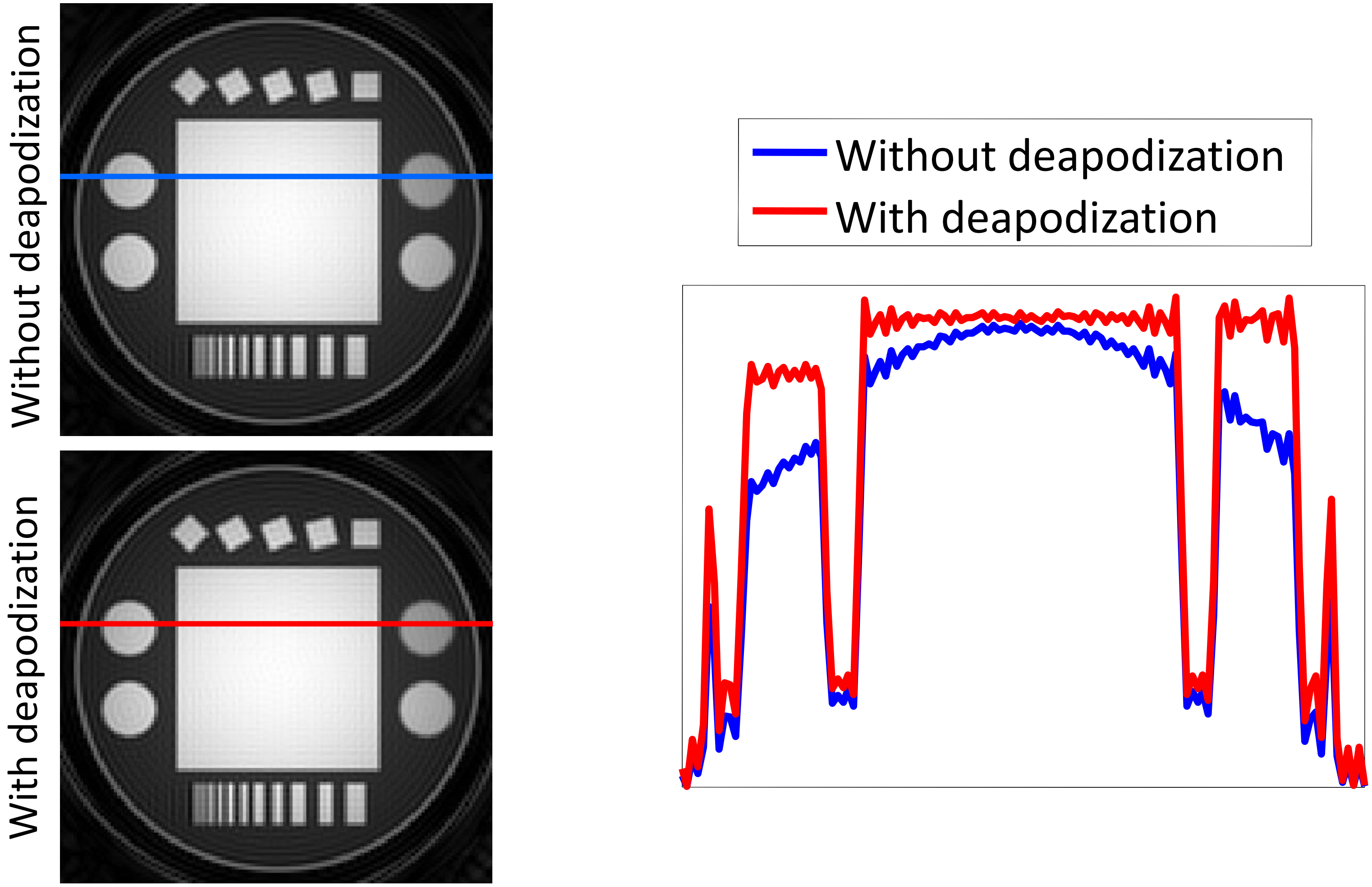

Gridding reconstruction steps

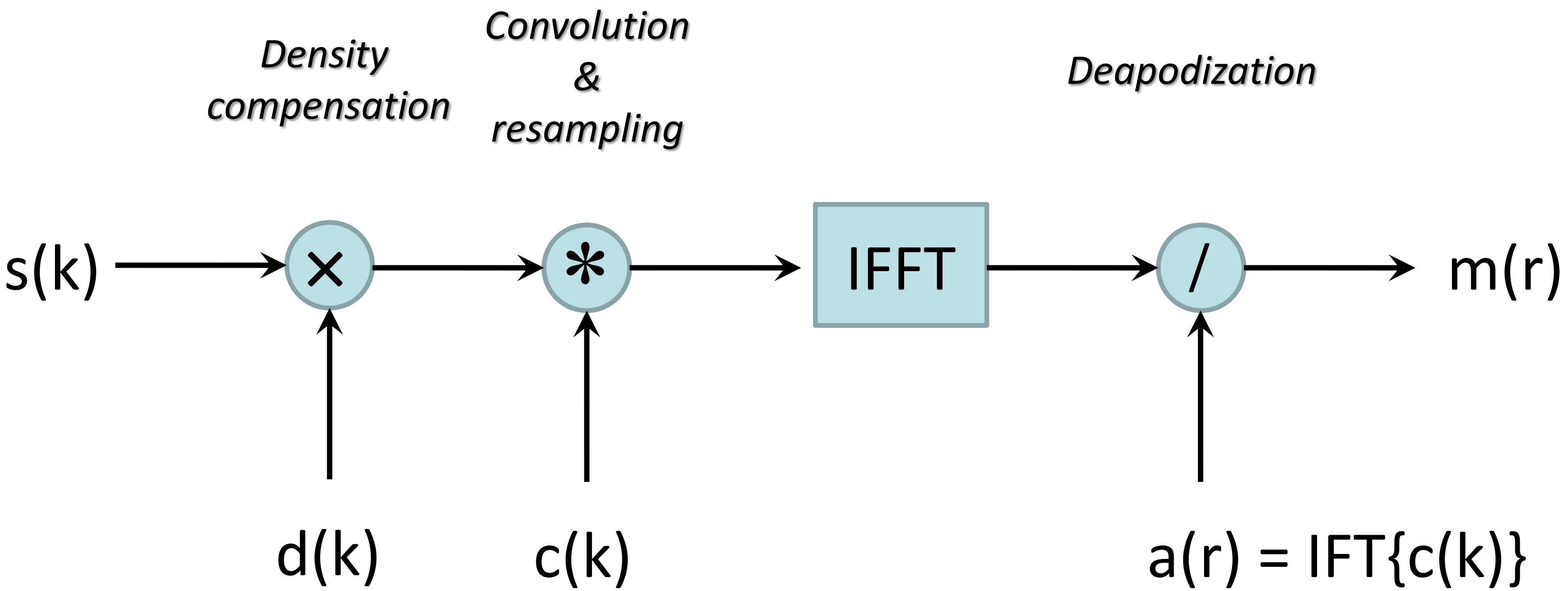

Summary of gridding reconstruction

- Compute the non-Cartesian k-space sampling pattern
- Choose the gridding kernel (e.g. Kaiser-Bessel)
- Density pre-compensation (if possible)
- Convolve the pre-compensated k-space data with the gridding kernel and evaluate the convolution at the Cartesian grid (oversampled)
- Apply inverse FFT
- Apply deapodization function
- Remove the oversampling by cropping the image

Non-Uniform FFT (NUFFT)

560 IEEE TRANSACTIONS ON SIGNAL PROCESSING, VOL. 51, NO. 2, FEBRUARY 2003

Nonuniform Fast Fourier Transforms Using Min-Max Interpolation

Jeffrey A. Fessler, *Senior Member, IEEE,* and Bradley P. Sutton, *Member, IEEE*

***Abstract*—The fast Fourier transform (FFT) is used widely in signal processing for efficient computation of the FT of finite-length signals over a set of uniformly spaced frequency locations. However, in many applications, one requires nonuniform sampling in the frequency domain, i.e., a *nonuniform FT*. Several**

argued compellingly for using trigonometric polynomials (complex exponentials) for finite-dimensional approximations in such problems [29] and proposed to use an iterative conjugate gradient reconstruction method with the nonuniform FFT

- Generalized version of the gridding algorithm
- Similar idea, but fast implementation
- Forward & adjoint operators (use in iterative algorithms)
- Several open-source implementations available
  - http://web.eecs.umich.edu/~fessler/irt/irt/nufft
  - https://github.com/andyschwarzl/gpuNUFFT
  - https://github.com/mmuckley/torchkbnufft
  - https://github.com/mikgroup/sigpy
  - https://github.com/mrirecon/bart